In Situ Pore Formation in Graphite Through Solvent Co-Intercalation: A New Model for The Formation of Ternary Graphite Intercalation Compounds Bridging Batteries and Supercapacitors

Gustav Åvall,* Guillermo A. Ferrero, Knut Arne Janßen, Moritz Exner, Youhyun Son, and Philipp Adelhelm*

For Li-ion and Na-ion batteries, the intercalation behavior of graphite anodes is quite different. While Li-ions intercalate, Na-ions only co-intercalate with solvent molecules from the electrolyte solution leading to ternary graphite intercalation compound (t-GIC) formation along with an expansion of the graphite interlayer spacing to 1.2 nm. This large interlayer spacing represents a micropore with parallel slit geometry. Little is known about t-GIC formation, but it is commonly believed that throughout the reaction the ion is accompanied by either a full or partial solvation shell. Here, it is elucidated for the first time, using two independent methods – mass measurements and electrochemical impedance spectroscopy – supplemented by operando microscopy, entropymetry and simulations, that the storage mechanism is far more complex. A new model for the electrochemical solvent co-intercalation process is proposed: As soon as solvated ions enter, the graphite structure is flooded with free solvents, which are subsequently replaced by solvated ions. Close to full sodiation, few free solvents remain and structural rearrangement take place to reach the full storage capacity. Thus, t-GICs represent a unique case of switchable microporous systems and hence appear as a bridge between ion storage in the bulk phase and in micropores, i.e., between batteries and supercapacitors.

1. Introduction

Electrochemical solvent co-intercalation reactions for rechargeable batteries have gained great attention in recent years after reversible sodium intercalation was accomplished in ordinary graphite using glyme-based electrolytes.[1] Although these systems so far show extreme volume expansion[2] and lower energy densities, they do offer far superior cyclability and enhanced charge transfer kinetics compared to conventional lithiumion and sodium-ion batteries (LIBs and SIBs).[3] Even though several papers have been published over the last years analysing the effect of different solvents and salts,[1,2b,4] as well as the reversible reaction having been identified for TiS$_2$,[5] some interesting fundamental questions have been unresolved such as how such a seemingly bulky and extreme reaction where the graphite undergoes a lot of mechanical stress can be reversible and fast, and how it can in some instances be energetically favourable over ordinary intercalation reactions. Already in the 1970s' the first articles on electrochemical solvent co-intercalations were published, with a focus toward material synthesis and primary energy storage applications, and several of those articles attempted to pinpoint the exact stoichiometry of what was being intercalated.[6] But, solvent co-intercalation was also of interest since the early 1990s' with regards to solid electrolyte interphases (SEI). Following the detection of small amounts of co-intercalated solvents in several carbonate based electrolytes, solvent co-intercalation constitutes the initial step in the SEI formation process in one of the two leading theories on SEI formation mechanism,[6c,7] even in electrolytes without glymes or propylene carbonate (PC) present.[8] Solvent co-intercalation is also a process of interest in the fields of electrical double layer formation and in confined electrolytes as the capacitance of an electrode grows greatly once the solvation shell and pore size becomes similar, and there is a continuous transition from non-Faradaic to Faradaic charge storage as the solvation

G. Åvall, G. A. Ferrero, K. A. Janßen, M. Exner, Y. Son, P. Adelhelm
Institut für Chemie
Humboldt Universität zu Berlin
Brook-Taylor-Str. 2, 12489 Berlin, Germany
E-mail: gustav.avall@hu-berlin.de; philipp.adelhelm@hu-berlin.de
P. Adelhelm
Joint Research Group Operando Battery Analysis (CE-GOBA)
Helmholtz-Zentrum Berlin
Hahn-Meitner-Platz 1, 14109 Berlin, Germany

shell becomes more and more confined.[9] Variations in the pore structure may further impact the storage mechanism and diffusion behaviour that further supports the fact that ion storage on the nanoscale can be a very complex process.[10] Reactions with reversible solvent co-intercalation seem to occur when the interlayer spacing of the host material is of similar size to the solvation shell, thus being an intermediate between double layer capacitors and batteries. Therefore, properties typical of both batteries and electric double layer capacitors are observed when such reactions occur.[3,9c,11] Thus, electrochemical solvent co-intercalation seems always present, leading to either successful SEI formation and subsequent intercalation of only bare ions, or in rare cases to reversible solvent co-intercalation.[11a] Therefore there is a broad interest in understanding this process and what enables it.

Even though many papers have recently been written about reversible solvent co-intercalation since the original papers in 2014,[1] the stoichiometry of the reaction is still unknown and under debate. Considering an electrolyte composed of an ether solvent (in particular glymes) and a sodium salt, the reaction with graphite has been expressed by many authors as:[1a,6a,c,7c,12]

$$[Na : G_x]^+ (l) + C_{20} (s) + e^- \rightarrow NaG_y C_{20} (s) + G_z (l), \quad x = y + z \quad (1)$$
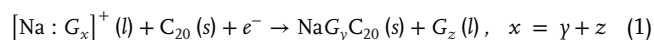
where G denotes a glyme molecule (diglyme (G2) the most investigated solvent), x is the number of glymes in the solvation shell, y the number of glymes coordinating the sodium inside the graphite and z are the number of glymes removed from the solvation shell during the reaction (also denoted "free" glymes). In practically all the cells assembled and reported on, the electrolyte solution was used in excess. This means that the carbon is the limiting reagent (typically ≈100 µL of electrolyte and ≈5–10 mg cm^{-2} graphite), making it possible to determine the ratio of carbon per Na$^+$ from the specific capacity.[1a] There is, however, no consensus on the number of glymes involved in the reaction. Two general schools of thought, however, can be identified: Partial desolvation (the process of removing solvents from the solvation shell) occurs in the reaction with $x \neq y$; or no desolvation occurs with $x = y$, and $z = 0$. To date, only a few papers have provided measurements on the number of solvents involved in electrochemical co-intercalation reactions.[2b,5b,6,13] For a sodium system with G2 as solvent, Kim et al. showed energy-dispersive X-ray spectroscopy as well as mass measurements where the mass change of the electrode at different voltages is compared with the pristine electrode mass.[2b] Based on their results, a G2:Na$^+$ ratio of 1 was determined. As a favourable coordination number ≈6 is often reported for Na$^+$,[14] the solvation shell is expected to consist of two G2 molecules, thus supporting the theory of partial desolvation.[2b] In either case, the prevailing model of solvent co-intercalation so far is that there is a constant reaction over the whole potential range where an ion either brings along its full or partial solvation shell. This, however, is in conflict with several experimental observations: i) Nuclear magnetic resonance (NMR) measurements do not report a linear increase in the signal from solvent molecules within the graphite with the state of sodiation (SOS), as recently reported by Escher et al., and free glyme molecules inside the graphite interlayer spacing were also detected,[15] ii) X-ray diffraction (XRD) clearly shows evidence of staging, yet the voltage profile does not display a sequence of plateaus, but instead a single one where additional so-

diation of the stage I compound occurs,[1] and clear pseudocapacitive features,[16] and iii) the macroscopic expansion observed in operando electrochemical dilatometry (ECD) does not correlate to the staging and expansion observed in XRD and changes with the SOS.[1b,17]

Herein we address the conundrum on the number of glymes electrochemically co-intercalated into the graphite host structure for monoglyme (G1) or G2 as the electrolyte solvents. By using several independent methods, we show that the reaction Equation (1) is too simple and inaccurate to describe the solvent co-intercalation process of glymes into graphite. We detect that the reaction changes drastically depending on the voltage, or SOS, in line with the results observed by ECD, XRD and the overall shape of the voltage profile, and also by the NMR studies that have reported on the presence of free glymes in the graphite.[15] We revisit the so-called mass difference experiment, which was carried out in previous studies, both recently and historically, and show that there is a systematic error in the measurement procedure due to a previously unknown instability of the system. Instead, we present an improved experimental protocol for the measurement of these mass changes to determine how many glymes are involved in the reaction. In addition, we have used in situ electrochemical impedance spectroscopy (EIS) to support the results from the mass measurements. Furthermore, these findings were also confirmed by means of entropymetry, to track changes in entropy of the system, and by operando microscopy to observe and follow the structural and color changes of the graphite electrodes. Finally, ab initio simulations were used to complement the experimental techniques. To conclude, we present a new model to describe the behavior of this system that is consistent with existing experimental results.

2. Results and Discussion

The common view on co-intercalation reactions is, that the number of co-intercalated solvent molecules per ion is always the same, irrespective of the state of charge.[2b,5b,6,13a,b] However, this is only a hypothesis and actually poorly supported by experimental data. As stated above, it is even unclear whether the complete or only parts of the solvation shell are co-intercalated. In an attempt to provide better experimental evidence, we have used several independent methods. In the following, we show that none of the methods is in support of this hypothesis and that a new model for the co-intercalation mechanism is required.

The co-intercalation reaction should lead to several measurable effects that can be used to study the amount of co-intercalated solvent molecules. First, if always the same number of solvent molecules are co-intercalated, there must be a linear mass increase of the electrode over time. Second, the co-intercalation of solvent molecules reduces the number of solvent molecules in the electrolyte solution. This means that the electrolyte salt concentration and hence its conductivity changes. The latter can be measured by EIS. The removal of solvent molecules from the electrolyte phase also causes a third effect, which is a decrease in electrolyte volume that can cause the cell to dry out. A systematic variation of the solvent volume should therefore allow the determination of how much solvent is co-intercalated.

**ADVANCED
SCIENCE NEWS**

www.advancedsciencenews.com

**ADVANCED
ENERGY
MATERIALS**

www.advenergymat.de

2.1. Mass Measurements

In early articles on solvent co-intercalation it was assumed that either a partial solvation shell with one G2 molecule, or a full solvation shell with two G2 molecules are co-intercalated with each Na$^+$ into graphite.[1a,2b] This was motivated by the coordination number of Na$^+$ that is typically reported to be 6.[14] Considering the general stoichiometry of the compound [Na:G2$_x$]C$_{20}$ with a maximum specific capacity $\approx$110 mAh g^{-1}$_{(graphite)}$, the mass ratios of the solvated ions ([Na:G2$_x$]) and the mass of graphite are 0.56 for $x = 1$, and 1.12 if $x = 2$. Therefore, by simply comparing the mass of the graphite electrode before and after sodiation, it should be easy to determine x, the glyme:Na$^+$ ratio.

As this approach appears quite straightforward, it has been carried out in several studies.[2b,5b,6,13a,b] We have reproduced some of these studies, see Figure S1a (Supporting Information), and indeed found a linear increase in mass indicative for $x = 1$.[2b] However, the analysis is oversimplified because the electrodes contain excess electrolyte, i.e., electrolyte on the surface and in the pores of the electrode, needs to be considered too. The common way reported to remove the excess electrolyte is to dry the electrodes before measuring the mass, but NMR measurements have already revealed that large changes occur in the sample during drying,[15a] – in fact, our analysis, using electrochemistry and XRD, Figures S1,S2 (Supporting Information), shows that the drying procedure removes all intercalated ions, strongly questioning the results previously reported. A comprehensive discussion is provided in the Supporting Information.

To extract more accurate information out of these measurements a more thorough analysis is needed. For a sodiated graphite electrode (SOS $\neq$ 0), its total mass m_{sod} (*measured immediately when taken out of the cell*) consists of three terms.

$$m_{sod} = m_0 + m_I + m_{exc} \qquad (2)$$

With m_0 being the mass of the pristine electrode, m_I being the mass of the intercalant, and m_{exc} being the mass of the excess electrolyte. In the desodiated state (SOS = 0) m_{desod} equals:

$$m_{desod} = m_0 + m_{exc} \qquad (3)$$

Now, the mass loss during the drying procedure can be due to changes in m_I and m_{exc}:

(a) Mass loss due to diffusion of solvated ions from the t-GICs to the surface and subsequent evaporation of solvent molecules and/or reactions between the charged species and the environment. The product of these processes is unknown but, e.g., NaOH could form in case of water impurities. Reactions with impurities can easily occur as the sodiated graphite is strongly reducing.

(b) The solvent in the excess electrolyte will evaporate. The result of this process is a loss in solvent molecules along with precipitation of the conductive salt (see Supporting Information).

Thus, after drying, the measured mass is not simply the sum of the intercalant and the pristine electrode, as previously assumed, but instead the mass of the 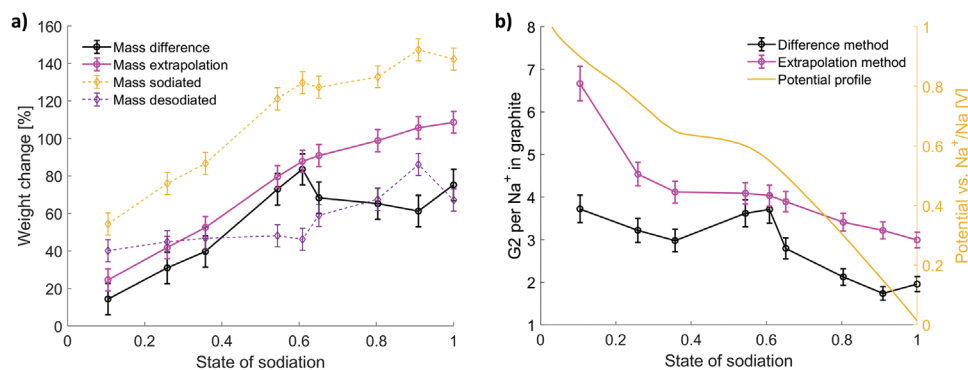pristine electrode and the end products of processes (a) and (b). This is important since it means that Equation (2) and (3) are only true immediately when the cell is opened, as both m_I and m_{exc} will evolve with time as the sample dries. Different from previous approaches, we therefore conducted time dependent measurement, where the mass of sodiated and desodiated samples are recorded over time, Figure S3 (Supporting Information) for details.

The mass of both the sodiated and desodiated samples initially decays exponentially, corresponding to process (b). However, while the desodiated sample quickly reaches a constant mass, the sodiated samples show a longer region characterized by a continuous, linear mass loss before eventually reaching a constant end value. (Figure S3, Supporting Information). As this linear decay in mass is only present in the sodiated samples, we ascribe it to process (a). Based on this observation, we devised two strategies to extract the mass of the intercalant from the mass measurement.

Mass difference method – Compare the masses of the sodiated and desodiated samples immediately when the cell is opened to exclude any time-dependent processes.

Extrapolation method – Extrapolate the linear decay of the mass of the sodiated samples, ascribed to process a), to time zero. See Figure S3 and discussion (Supporting Information) for more details.

In the G2-based electrolyte, there is a very large increase in the mass immediately when sodiation starts (at high potentials, i.e., low SOS), **Figure 1**a. The mass then increases approximately linearly until the main voltage plateau (SOS = 0.4–0.6), where a sharper increase in mass is seen. After this, entering the pseudocapacitive region, the mass change seems to stabilize. As expected, the mass of the desodiated samples is always lower than the one of the sodiated samples, and highly dependent on the SOS it has been cycled to, suggesting a partially irreversible effect on the electrode. Importantly, there is a very large mass change already at low SOS which indicates that intercalating just a few solvated ions is enough to cause significant structure changes, see Figure 1a. These mass changes are then almost constant until the plateau ends after that it starts to increase again. Figure 1a also shows that both the mass difference method and the extrapolation method exhibit similar trends. Calculating the G2:Na$^+$ ratio in the graphite host structure (see Figures S4–S8 and Tables S1–S4, Supporting Information) shows, that as the first solvated ions enter the graphite galleries, the structure is flooded with free G2 molecules as the G2:Na$^+$ ratio is much greater than 2, see Figure 1b. After this, the G2:Na$^+$ ratio in the graphite drops, presumably as free G2 molecules are preferentially replaced by solvated ions, until the main plateau is reached. This plateau coincides with the formation of the stage I compound[2b] and is a region with a large increase in mass (Figure 1a) and with a relatively stable G2:Na$^+$ ratio. Once the stage I compound is formed, the reaction appears pseudo-capacitive and the G2:Na$^+$ ratio decreases, i.e., free solvent molecules are again replaced by solvation shells. Finally, at 0.15 V versus Na$^+$/Na, where an ordering takes place (observed in XRD and reported as an in-plane superstructure),[2b] there seems to be a small increase of the G2:Na$^+$ ratio. This indicates that new room has been created in the expanded graphite lattice that is again filled with solvated ions. The final stoichiometry of the compound is consistent with fully solvated ions [Na:G2$_2$]C$_{20}$ in addition to some free solvents inside the graphite, i.e.,

**ADVANCED
SCIENCE NEWS**

www.advancedsciencenews.com

**ADVANCED
ENERGY
MATERIALS**

www.advenergymat.de

Figure 1. Mass measurement results. a) Weight change of electrodes immediately after cycling (dashed yellow) in 1 M NaPF$_6$ in G2 to different states of sodiation (SOS), results for the desodiated control samples (dashed purple) and mass changes due to the intercalant calculated with the mass difference method (black) and the extrapolation method (magenta). b) The number of G2 per Na$^+$ in graphite calculated by the mass difference method (black) and the extrapolation method (magenta), as well as the voltage profile (yellow). Error bars were calculated with the standard formula for propagation of errors from the mass measurements.

slightly more than 2 G2 per Na$^+$, as has been suggested in NMR studies.[15] Similarly, in a G1 based electrolyte there is a large mass change at the initial stages of sodiation that correlates to a large G1:Na$^+$ ratio, Figure S8 (Supporting Information), showing that this feature is not exclusive for G2. Nevertheless, the G1:Na$^+$ varies less than the G2 counterpart with a final stoichiometry slightly higher than [Na: G1$_3$]C$_{20}$, i.e., fully solvated Na$^+$ with some free G1. Most importantly, while the capacity for both electrolytes is identical, the amount of solvent being co-intercalated is different and is a function of the SOS, and the final stoichiometries appears to be consistent with fully solvated Na$^+$ in addition to some free solvents in the graphite structure. At low voltages, and similarly to the G2, there seems to be some sort of structural rearrangement also in the G1-based electrolyte allowing more glymes to enter the structure. Even though the reproducibility of the data is high, we found the uncertainty in the weight changes to be within ±5.9%, we refer the reader to a detailed discussion of errors in the Supporting Information.

We draw several conclusions from these mass measurements: *i)* In contrast to the existing belief, the G2:Na$^+$ ratio (and more generally the glyme:Na$^+$ ratio) is not constant throughout the intercalation reaction but changes dramatically during sodiation. *ii)* Graphite is flooded with free glyme molecules as soon as the first solvated ions enter the structure. *iii)* In the fully sodiated state, the glyme:Na$^+$ ratio is slightly higher than 2 for G2 and 3 for G1, i.e., the graphite is mostly filled with solvated ions but there is also free solvents left inside the graphite, as reported in several NMR studies.[15]

Overall, these findings clearly show that the existing view on how solvent co-intercalation reactions with graphite take place needs to be reconsidered. We therefore applied several more methods to understand and corroborate the reaction mechanism, eventually enabling us to suggest a new reaction model.

2.2. Electrochemical Impedance Spectroscopy (EIS)

In normal intercalation batteries, the amount and composition of the electrolyte is constant because formally only ions are shuttled between the electrodes. This is not the case when solvent co-intercalation occurs. Co-intercalation of solvent molecules during sodiation of the graphite causes a decrease in the amount of solvent in the electrolyte phase (the opposite occurs during desodiation). This means that the electrolyte volume and concentration change during cycling. This effect can be clearly seen when working with highly concentrated electrolytes,[25] or when limiting the electrolyte volume, as the reaction can suddenly stop when the cell dries out (vide infra, Figure S11, Supporting Information). The degree in volume and concentration change depends on how many glymes are involved in the redox reaction and on the initial electrolyte to electrode ratio. Knowing the initial salt concentration, the electrolyte volume used and the mass of the active material, the number of glymes involved in the reactions can be deduced if the salt concentration of the electrolyte can be monitored during cycling. We therefore used in situ EIS for determining the bulk resistance of the electrolyte by analyzing the high frequency region of an impedance spectrum. This resistance is related to the conductivity of the electrolyte and is hence sensitive to changes in the salt concentration. Since standard molar concentrations (1 M) lead to small resistance variations that cannot be monitored with enough precision, we selected very low starting concentrations where the conductivity is low due to a lack of charge carriers and the changes are more intense. The initial resistance was measured for different initial concentrations (0.05–0.15 M), showing a very strong and clear concentration versus resistance trend, **Figure 2**a and Figure S10 (Supporting Information), enabling a resistance from an EIS measurement to be mapped to the electrolyte concentration for various SOS. By knowing the initial molar salt concentration of the electrolyte, the amount of glymes inside the graphite can be calculated. Doing so for three G2-based electrolytes, with starting concentrations of 0.075, 0.1, and 0.125 M, we observed a large drop in the resistance at the beginning of sodiation and on the plateau, Figure 2b. This analysis shows that there is a large amount of G2 molecules entering the graphite immediately at the start of sodiation and on the main plateau, Figure 2c, while there is a net flow of G2 molecules out of the graphite in the pseudocapacitive voltage region. Computing the G2:Na$^+$ ratio, Figure 2d, shows that there are many more solvents in the graphite at low SOS than fits in the solvation shell of the thus far intercalated sodium. The G2:Na$^+$ ratio then decreases until the plateau is reached where the ratio becomes constant, or possibly increasing a bit, after that it declines sharply again.
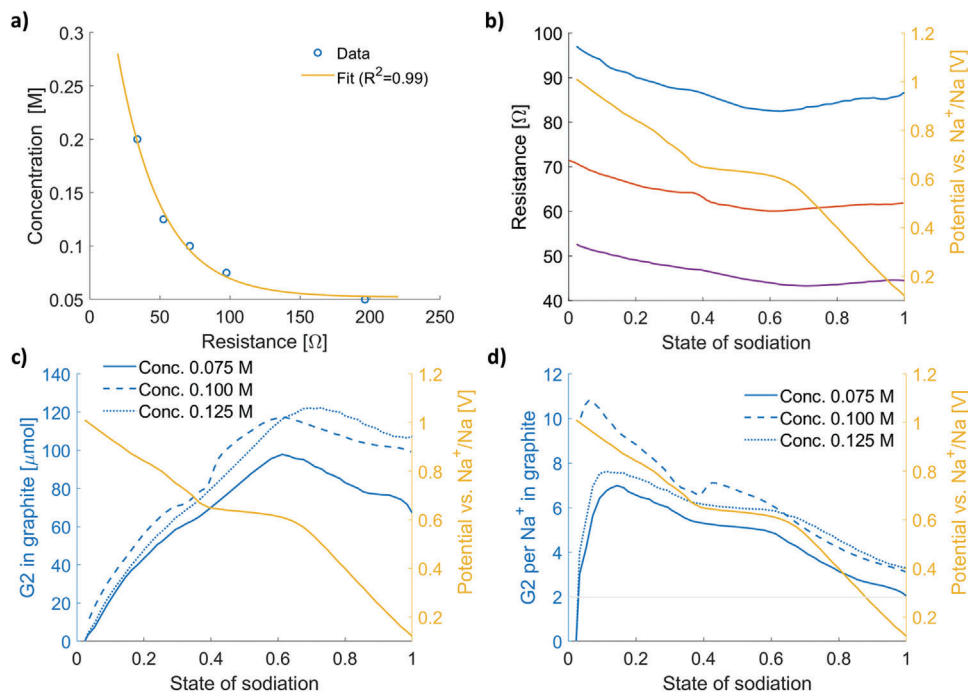
Figure 2. EIS measurement results. a) Calibration data used to map a resistance to a concentration. b) Bulk electrolyte resistance of a G2 based electrolytes as a function of sodiation for electrolytes with 0.075, 0.1, and 0.125 M NaPF$_6$. c) The mols of G2 in graphite as function of mols of Na$^+$ intercalated. d) The overall G2:Na$^+$ ratio inside of graphite.

Thus, the impedance measurements corroborate the results of the mass change measurements, and the same conclusions can be drawn: The reaction changes drastically depending on the state of sodiation and the graphite appears to be flooded with glymes as soon as sodiation starts. The glyme:Na$^+$ ratio then drops as free glymes are preferentially replaced by solvated ions until the main plateau where again there is a huge flux of glymes into the graphite, see Figure 2c,d. In the pseudocapacitive region, the reaction starts to stabilize and the final ratio of G2:Na$^+$ is $\approx$2–3, indicating that the Na$^+$ in the graphite is fully solvated with some free solvents remaining.

One might argue that the large change in masses measured in the mass measurement analysis can be caused not by glymes entering between the graphite layers, but instead due to the electrolyte solution filling into the graphite expanded surface. The impedance measurements, in good agreement with the mass measurements, rule out this possibility. Since these measurements are sensitive to the bulk electrolyte resistance, the ratio of glymes to salt is detected in-situ. If the graphite was being filled with electrolyte, the overall concentration in the electrolyte would not be altered. Increases in the electrolyte concentration can only be caused by a preferential removal of solvents.
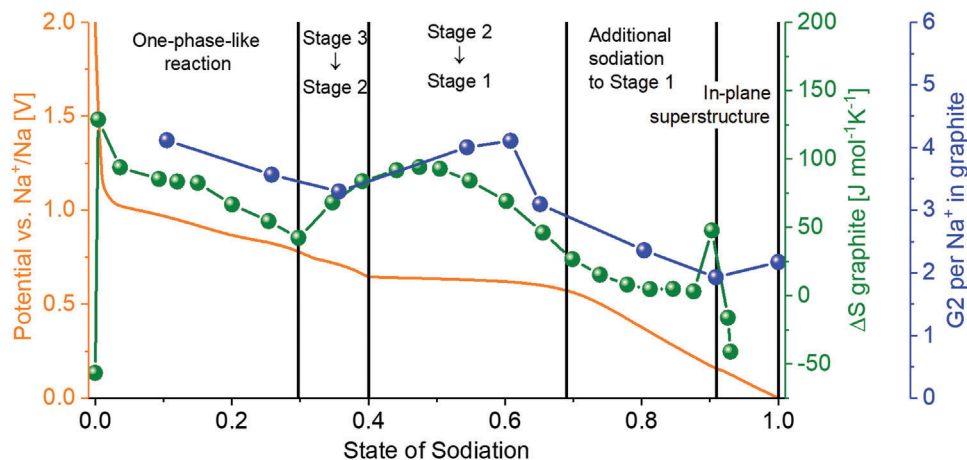
2.3. Alternative Methods

2.3.1. Glyme Limited Cells

In lab experiments, usually far more electrolyte is used in standard coin cells (100 μL) than what is needed to fully sodiate the graphite through the co-intercalation reaction and hence in a

standard setup the graphite is the limiting reagent, i.e., the redox reaction ends when there is no carbon left to react. Thus, when normalizing by the graphite mass, similar specific capacities are found from which the amount of carbon atoms involved in the reaction can be determined. If instead, the glyme is the limiting reagent it would be possible to deduce the amount of glymes involved in the reaction. To study this, we constructed two different types of setups, see Supporting Information for details, where the glyme is the limiting reagent. In the first setup, the electrolyte volume is maintained constant for different salt concentrations while in the second one the volume added is varied for a defined initial salt concentration. In the case of G1, both methods showed that $\approx$3.2 G1 molecules are co-intercalated along with each Na$^+$, Figure S12 (Supporting Information), which supports our previous findings that again at full sodiation, the Na$^+$ is not only fully solvated by glyme molecules but there are also small amounts of free solvents present. Similar experiments with G2 based electrolytes did not produce any trustworthy results, see Supporting Information for discussion.

2.3.2. Entropymetry

Recent articles have highlighted how entropymetry can be used to study structural changes in the electrode as well as changes in electrolyte composition.[26] In a normal half-cell setup, changes in entropy ΔS can be ascribed to changes in the number of possible lattice configurations of the intercalated ions in the electrode. As such, structural transformations can be monitored as a function of SOS by simple temperature-dependent electrochemical measurements using a climate chamber. For these experiments,

**ADVANCED
SCIENCE NEWS**

www.advancedsciencenews.com

**ADVANCED
ENERGY
MATERIALS**

www.advenergymat.de

Figure 3. Results from entropymetry a) Comparison of the potential with the entropy variation and the G2:Na$^+$ ratio from the mass difference measurement.

the cell is paused at fixed intervals and the changes in OCV are measured with the temperature variation, see Supporting Information for details on the procedure. We monitored the changes in entropy at different SOS achieved by intercalating sodium at low current densities (10 mA g^{-1}). The change of OCV during the temperature change was then used to calculate the entropy change. All the experiments were made in a half-cell configuration with Na-metal as reference and counter electrode. In order to discard the contribution of sodium, the entropy of the sodium metal was subtracted from the final result.[27] Normally, as discussed, in such a setup the entropy variations are only due to changes in the electrodes. This, however, relies on solvation and desolvation happening simultaneously and is hence not true when solvent co-intercalation occurs. As the desolvation step is missing for co-intercalation reactions, these measurements will be sensitive to entropy changes in the electrolyte as well as the electrode. In symmetrical cells, where the two electrodes are in contact with different electrolytes, Wang et al. were able to measure the relative entropy changes between the electrolytes due to solvation effects, showing that entropy changes in the electrolyte are orders of magnitude larger than the entropy changes in the electrodes.[26b] This is not surprising, given that the electrodes are crystalline structures and hence there are a lot fewer allowed configurations of atoms compared to a liquid. Thus, the entropy changes measured for the co-intercalation reaction should be dominated by the entropy changes in the electrolyte.
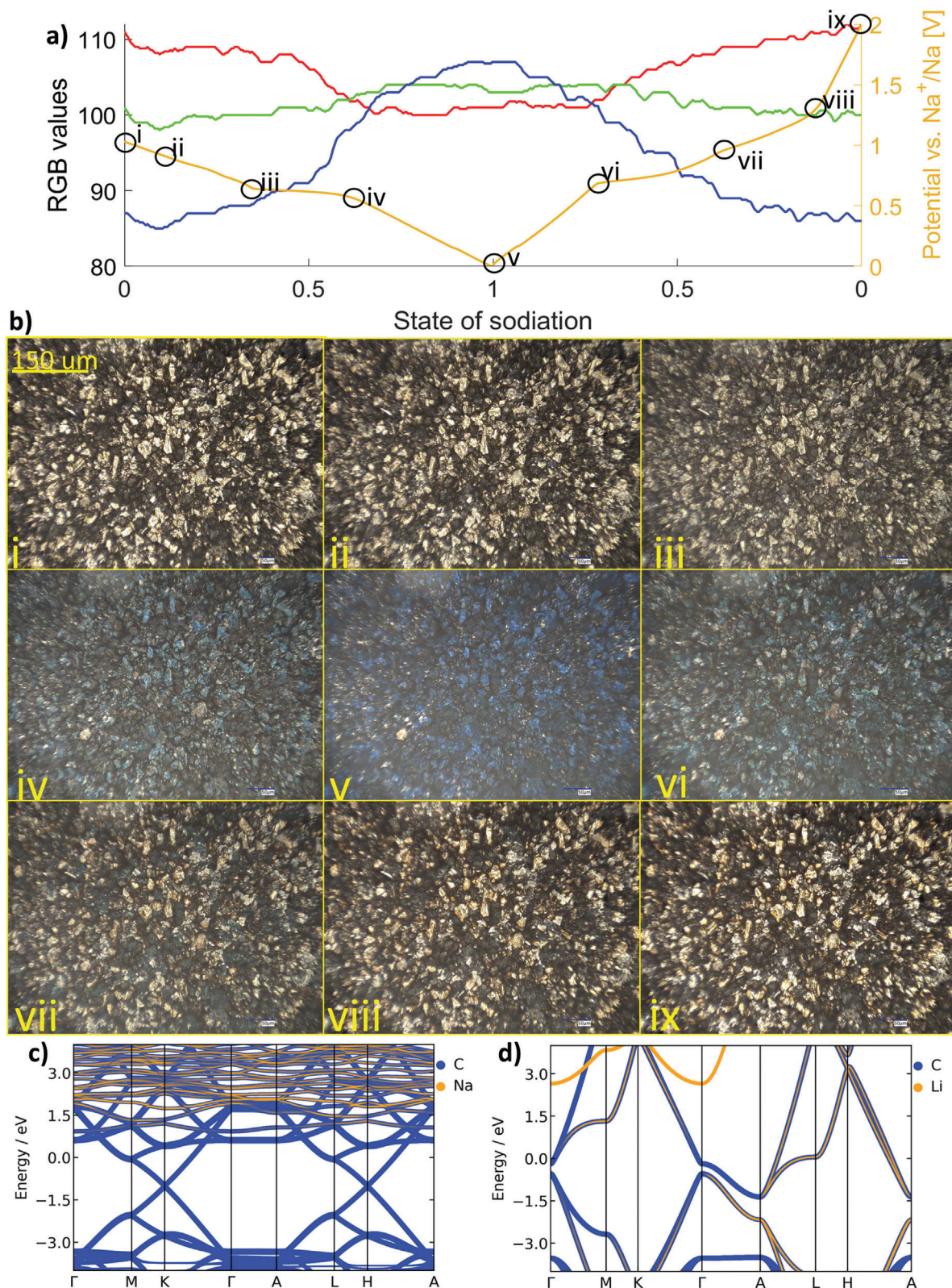
Figure 3 displayed the variation of the entropy when sodiated along with the capacity profile, while the lines mark the change in staging obtained by XRD when using G2 as solvent.[2b] There is a huge increase in the entropy change at the beginning of sodiation, as well as on the plateau, where the mass measurements and impedance measurements show that a large amount of glymes are entering the graphite. As the graphite is being opened by the solvated ions, they also open the graphite structure for free solvents to enter. Thus, the available volume for free solvents increases, i.e., the microstate in the liquid is available just as before, but there are now also possible microstates for solvated ions and free solvents inside the graphite lattice causing a huge rise in entropy, here detected as large positive value of ΔS. In the pseu-

docapacitive region where the impedance measurement shows a constant resistance, the $\Delta S \approx 0$ indicates there is no change in available microstates. At this point, both XRD and dilatometry shows that the graphite is fully opened, and hence no new space for solvated ions and free solvents can be created.[2a,b,17a] At 0.15 V versus Na$^+$/Na there is a quick jump in the ΔS value and then it becomes negative. A negative ΔS shows that the available microstates are decreasing, which here coincides with a detection of a final in plane superstructure formation in XRD.[2b] As the system is filled almost only with solvated ions, the number of available microstates for free solvents drastically decrease as the solvated ions take on a closer packing to reach the full capacity of the system, see Supporting Information for detailed discussion. Figure S13 (Supporting Information) displayed similarly the results obtained when G1 was used as the solvent. In this case, we observed a similar increase on the entropy change at low states of sodiations followed by a constant decrease when sodiation continues. Before the voltage plateau there is a change on the entropy variation that can be correlated to the beginning of the stage 1. After that, and similar to the mass analysis, there is a constant drop on the entropy calculated.

2.3.3. Color Evaluation

It is well known that when Li$^+$ is intercalated into graphite it alters the band structure, which in turn changes the optical properties of the material turning it golden orange at full lithiation.[28] Similarly, there should be substantial changes to the band structure of graphite when solvated ions are intercalated as the structure is greatly distorted. Hence, the reaction should have a clear effect on the color of the graphite. Using operando microscopy, the Red, Green and Blue (RGB) value of each pixel was analyzed and tracked during sodiation and desodiation. Immediately upon sodiation, there is a drop in intensity of all RGB values, **Figure 4**a and Figure S14 (Supporting Information). We attribute this to a large initial expansion of the graphite surface when the glyme molecules are flooding the graphite leading to a much greater quantity of light being absorbed per cross sectional area. After

ADVANCED
SCIENCE NEWS

www.advancedsciencenews.com

ADVANCED
ENERGY
MATERIALS

www.advenergymat.de

Figure 4. Results from optical measurements a) voltage profile with RGB values and b) with microscopy figures of the sample. c) the band structure of $[Na:G2_2]C_{32}$, and d) of LiC_6 where the orbital contribution of carbon (blue) and Na/Li (yellow) has been projected, where the bands have been shifted by the respective systems Fermi energy.
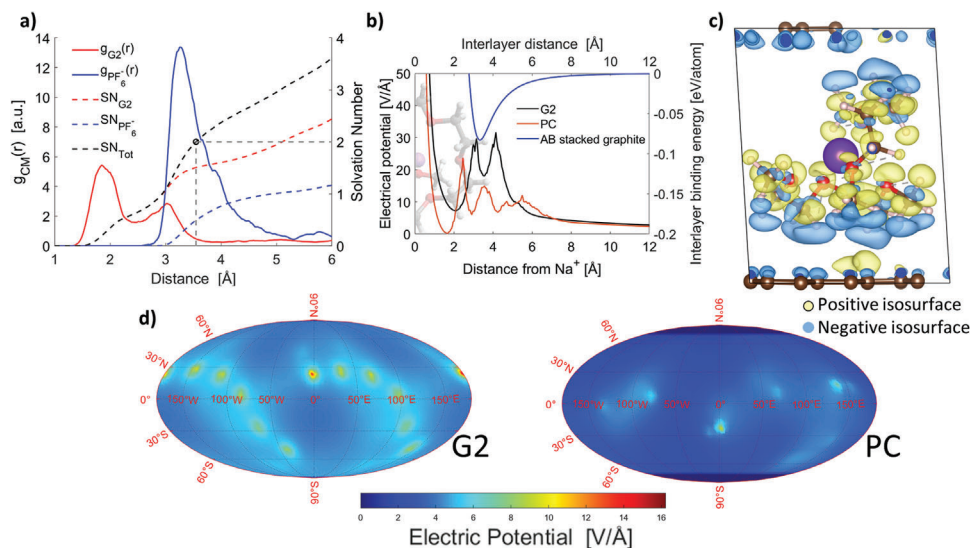
Figure 5. Results from ab initio molecular dynamics a) The CM RDFs with respect to G2 (solid, red) and the PF_6^- (solid, blue) as well as their SNs (dashed lines) and the total SN (black, dashed), b) the electrical field strength at a distance from Na^+, averaged over the entire sphere around G2 (solid black) and PC (orange), as well as the interlayer binding energy of AB stacked graphite (blue). c) The electron density difference of a stage I t-GICs with G2 with blue (decrease in electron density, more positive) and yellow (increase in electron density, more negative) 0.3 e $Å^{-1}$ isosurfaces drawn. d) the Mollweide projection of the electric field averaged along solid spherical angles of G2 (left) and PC (right), note the atoms of the solvent molecules can be identified by the bright spots in the figures.

this initial drop in brightness, the average amount of blue in the sample steadily increases. Once the plateau is reached, there is a very sharp increase in blue and a decrease in red, and a minor decrease in green, causing the graphite to turn blue in clear contrast to orange color of LiC_6, Figure 4 and Figure S15 (Supporting Information). The sample color then turns into an even deeper blue until full sodiation is reached. The desodiation proceeds in the opposite order. Similar results are also seen when a G1 electrolyte is used, Figure S16 (Supporting Information). Comparing the band structures of LiC_6 and $[Na:G2_2]C_{32}$, Figure 4c,d, we see that the energy bands are much less separated in the case of $[Na:G2_2]C_{32}$, indicating that more red light can be absorbed, and there is a large continuum of available bands coming from the intercalant. Computing the optical absorbance, Figure S17 (Supporting Information), LiC_6 absorbs light in the blue region of the visual spectra, while $[Na:G2_2]C_{32}$ has a clear broad peak in the infrared-green region, and lower absorbance in the blue part of the visible spectra compared to LiC_6. There are also other large changes in the band structure, for instance at the Γ-point in $[Na:G2_2]C_{32}$ has a large band gap, while LiC_6 is almost gapless. Similarly, at the K-point $[Na:G2_2]C_{32}$ is almost gapless, while LiC_6 shows a large band gap. The Li orbitals also contribute significantly to the bands close to the Fermi level (here shifted to 0 eV), while Na orbitals only contribute to bands 1.5 eV or higher than the Fermi level, however, the oxygen and hydrogen on the G2 molecules contribute to several bands close to the Fermi level, indicating they are interacting more with the graphite than the Na^+. Although, it should also be noted that the color changed might not be due to the presence of the solvents, as lithiated graphite also appears blue at low levels of lithiation ($\approx LiC_{20}$). The color of lithiated graphite, however, has previously been reported to correlate to the staging of graphite, but sodiated graphite turns blue first when a stage I

compound is formed, while lithiated graphite is golden at stage I formation.[28]

In the cell setup for the operando microscopy only the edges of the graphite electrode are in contact with the separator. Looking at the edge region, transport toward and into the graphite during first stages of sodiation and before the main plateau is observed. This again shows that there is a very large flow of electrolyte volume into the graphite immediately upon sodiation. Upon desodiation, once on the main plateau, a flow out of the graphite back into the separator is observed. Moreover, the breathing motion reported by Escher and Goktas et al. is very clearly seen, see Figure S15 and Videos (Supporting Information).[2a,17a]

2.4. Theoretical Considerations

The local electrolyte structure in a 1 M $NaPF_6$ in G2 electrolyte was studied using Car-Parrinello Molecular dynamics. The cation centred partial radial distribution functions (RDFs), calculated with respect to oxygen and fluorine, but also with respect to the centre of masses (CM) of the solvents and anions, shows that the solvation shell is mostly composed of oxygen/solvents but there is also a presence of fluorine/anions, **Figure 5** and Figure S18 (Supporting Information). The integrated RDFs shows a coordination number of ≈ 6 and a solvation number (SN) of ≈ 2 in the G2 based electrolyte, which is expected for Na^+.[14] The SN, however, is not static as often pictured with a stable well-formed solvation shell, but is highly dynamic. Many solvation shells have only partially coordinated glyme molecules, identified by the CHAMPION software, Figure S19 (Supporting Information),[29] which can also be seen in the CM partial RDFs were two clearly distinguishable peaks are seen for the G2-CM, Figure 5a. This is usual in conventional electrolytes as the environment around a solvation shell is

**ADVANCED
SCIENCE NEWS**

www.advancedsciencenews.com

**ADVANCED
ENERGY
MATERIALS**

www.advenergymat.de

Table 1. The interactions that determine whether b-GIC or t-GIC formation is possible.

	Distorting lattice	Graphite-intercalant interaction	Intercalant-Intercalant interaction	Desolvation
b-GICs	Small cost	Large gain	Large cost	No cost
t-GICs	Large cost	Small gain	Small cost	small gain

dynamic and there is often a fast exchange between the first and second solvation shell.[14h,j,30] Comparing the CM RDFs with the partial RDFs shows that the atomic RDFs have much more clearly defined plateaus, while the CM RDFs are more continuously increasing, showing that the first and second solvation shell are often connected by a bridging glyme molecule that only partially coordinate the cation. Thus, when a solvated ion is intercalated, it is not unreasonable that it will bring along all solvents that are at the moment coordinated to it. Moreover, as the solvent molecules are connecting the first and second solvation shell, there is a large interaction between them, and hence also parts of the second solvation shell might move along with the first solvation shell into the graphite. Taking the radius of the solvation shells as the furthest distance between the Na^+ and a hydrogen atom of a fully coordinated G2, plus the van der Waals radius of hydrogen, a solvation shell with 2 fully coordinating G2 molecules has a radius of 5.5 Å. Note that the solvation shell is a priori larger than a single solvent molecule, and as the interlayer distance in fully sodiated graphite is reported to be between 11.6–11.9 Å,[2b] there should be ample space for free solvents to move in between the graphite layers. In fact, such a large interlayer distance can be considered as a micropore.[31] Compared to a solvation shell with 6 PC molecules, with a radius of 8.8 Å, the glyme based electrolyte produce significantly smaller solvation shells and hence the expansion of the graphite lattice would not have to be as severe in G2-based electrolytes compared to PC-based, given that full solvation shells are intercalated, Figure 5b. The interlayer binding energy of graphite, however, is already close to 0 at the interlayer distances required, and observed, when co-intercalation occurs, see Figure 5b. This indicates that the graphite would delaminate and fall apart at room temperature unless the sheets were held together by the intercalant. AB and AA stacked graphite are degenerate at these distances, Figure S18 (Supporting Information). As both even and odd (00l) peaks are visible in XRD, graphite is able to transform from AB stacked in the pristine state to an AA or a combination of AA and AB stacking when reversibly intercalating solvated ions.[2b,11b] Given that stacking is still present in the expanded system, there is a translational symmetry along the c-axis in the expanded graphite unit cell and hence the graphene sheets are not completely free to slide relative to one another. Again, as the interlayer binding energy at these extreme interlayer distances is ≈0, and much lower than the thermal energy at room temperature, the fact that the structure does not delaminate, and even keeps translational symmetry along the axis of expansion can only be explained by it being kept together by the intercalant. This can also be seen looking at the charge density change of graphite with intercalated solvated ions, Figure 5c, where electron density is being pulled not only from the graphite layers but also the hydrogen atoms (blue, negative electron density difference isosurfaces) into the interior of the solvation shell (yellow, positive electron density difference isosurfaces), ending up

mostly around the oxygen and carbon atoms close to the central cation, but also some electron density moves to regions between the graphite layers and the closest hydrogen, previously reported by Jung et. al.[32] – This shows that the interaction between the Na^+ and the negatively charged graphite is highly indirect and is mediated by the solvent molecules that have been polarized by their contact with the Na^+.

Expanding the structure even more to accommodate a PC-based solvation shell would cost no additional energy, and hence one might believe that the size of the solvation shell would not make a difference as the structure is already expanded well beyond its limits. The size of the solvation shell, however, has a strong influence on the electric field around the solvation shell; the electric field strength is significantly larger just outside a glyme based solvation shell, 8.5 V Å^{-1} in the case of G2, compared to 3.3 V Å^{-1} for PC, Figure 5b. Well outside the solvation shells, the fields are equal according to Gauss's law, as they still only contain a charge of +1. A Mollweide projection of the electric field averaged along solid spherical angles, extending from the hydrogen atom furthest from the Na^+ to a van der Waals radius of hydrogen and carbon, i.e., approximately the distance between the solvation shell and the graphite layer, also shows that the electric field is much stronger around the solvation shells composed of glymes instead of PC molecules. Hence, a smaller solvation shell would have a greater ability to hold the graphene sheets together. Thus, for the structure to remain intact a smaller solvation shell, with stronger electrical fields around it, is preferable, especially if the structure is to retain its crystallinity along the c-axis. Larger solvation shells would not interact as strongly with the graphite layers and the structure would risk delaminating, as observed when PC-based electrolytes are used alongside graphite. These forces between the graphite and the solvation shell, although necessary, are smaller compared to the forces in normal b-GICs where the graphite lattice is in direct contact with the cation.

For the solvent co-intercalation reaction to occur, there must be a balance between the cost of expanding the graphite structure, and the attraction between the graphene sheets and the solvation shell, as well as the repulsion between positively charged solvation shells, but also the gain of not expending energy in the desolvation process. In complete analogy with what occurs in ordinary b-GICs, where there must be a balance between the comparatively small cost of expanding and distorting the graphite lattice, the desolvation process and the attraction between the ion and the graphite, and the repulsion between ions. Energetically, however, the reactions forming b-GICs and t-GICs are in complete opposite, Table 1. There is a large cost for expanding the lattice, in the case of a t-GIC, but small for a b-GIC, but in a b-GIC the graphite-intercalation attractive forces are much larger than in a t-GIC due to the much closer proximity of the bare ions to the graphite sheets compared to the solvated ions. As the repulsion between intercalated solvation shells in t-GICs is small compared

**ADVANCED
SCIENCE NEWS**

www.advancedsciencenews.com

**ADVANCED
ENERGY
MATERIALS**

www.advenergymat.de
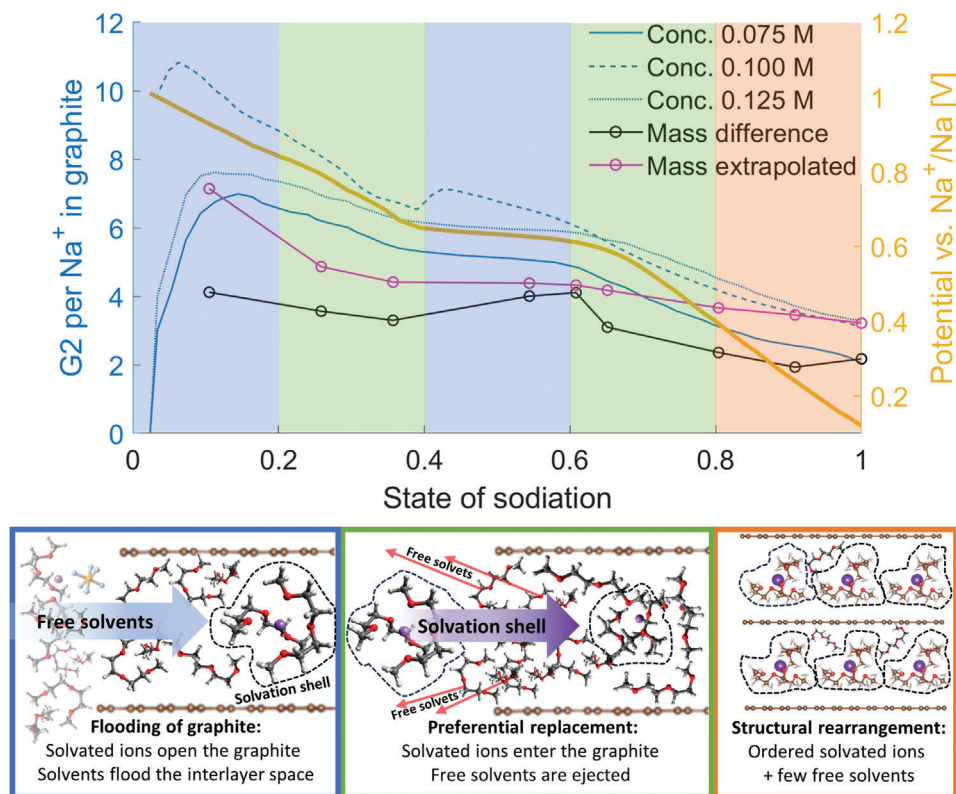
Figure 6. New model for solvent co-intercalation. The voltage profile along with the G2 per Na$^+$ measured with the mass experiments (circles) and EIS (blue lines), Figures 1b and 2d, along with a schematic illustration of flooding of the graphite, the preferential replacement of free solvents by solvated ions, and structural rearrangement into a more ordered structure. Solvation shells are encircled by dashed lines, and the coloured region in the voltage profile matches the coloured boxes with the schematic process.

to the repulsion between bare ions in b-GICs, it has a less detrimental effect on the stability of the system. Finally, there is a gain from bypassing the desolvation step in the formation of a t-GIC, but this has no net effect on the equilibrium potential of b-GIC formation but does influence the kinetics of the reaction.

All of these energies have to be assessed for each individual system. But the energy difference between a t-GIC and b-GIC due to the desolvation process is known and is equal to the solvation free energy of that particular electrolyte. While in a b-GIC the dependency of the redox reaction on the desolvation process is never observed due to the simultaneous solvation process at the counter electrode, the redox reaction in a t-GIC will be directly dependent on the solvation free energy of the electrolyte.

2.5. Comparison and New Model for Solvent Co-Intercalation

Comparing the results of the mass measurements and the EIS concentration measurements, **Figure 6**, they show the same trend and are even in good quantitative agreement in the pseudocapacitive region. Together, they give a complete picture of the entire reaction process: The first solvated ions that intercalate the graphite open the structure causing a large interlayer spacing that solvents flood into. As there is no electrochemical drive to intercalate free solvents, solvated ions are preferentially intercalated and free solvents will be ejected out of the graphite to make room for

the solvated ions and thus the glyme:Na$^+$ ratio steadily decreases until the plateau region. In this region, the final layers are opened up which are again flooded by free solvents (formation of a stage I compound), and then the process repeats where the free solvents are steadily replaced by solvated ions. In the non-faradaic region, it seems that most of the free solvents in the graphite are ejected while the solvated ions continue to be co-intercalated and re-arrange inside until the graphite reaches its full storage capacity. This new model for solvent co-intercalation reactions is illustrated in Figure 6.

3. Conclusion

By combining several independent experiments, we find that solvent co-intercalation into graphite is a process that is far more complicated than previously anticipated. By ex situ mass measurements and in situ EIS we show that the number of solvent molecules being intercalated per Na$^+$ turns out to depend on the state of sodiation. We observe that as soon as the first solvated ions are intercalated, they expand and open the graphite structure essentially making the graphite interlayer spacing a large pore for free glyme molecules to enter. During this stage of sodiation a very large amount of solvent molecules flood the graphite interlayer spacing but due to the highly charged environment, anions are left behind in the bulk electrolyte. The free solvent molecules are then slowly replaced by solvated ions. This process of

**ADVANCED
SCIENCE NEWS**

www.advancedsciencenews.com

**ADVANCED
ENERGY
MATERIALS**

www.advenergymat.de

flooding the structure with free solvents and then replacing them with solvated ions then repeats during the main voltage plateau as the structure fully expands and opens up to form a stage I compound. At low potentials, structural rearrangement into the final structure occurs, which consist of mostly fully solvated ions with a few free solvent molecules still present.

Finally, we want to emphasize the fact that the discussed reaction mechanism is also intriguing from the viewpoint of porous materials and supercapacitors. The opening of the (non-porous) graphite structure by solvated ions leads to an interlayer distance of ≈1.2 nm, i.e., a distance commonly classified as a micropore. The opened graphite structure represents an ideal parallel slit pore. Flooding of such micropores by free solvents is, as also supported by our calculations, quite reasonable. To the best of our knowledge, the formation of t-GICs is the only process that shows such a highly defined in-situ generation of microporosity. Moreover, the process is switchable as the graphite structure is recovered during desodiation. Solvent co-intercalation reactions could therefore build a true bridge between ion storage in the bulk phase and in micropores, i.e., between batteries and supercapacitors.

4. Experimental Section

Electrode and Cell Preparation, Cell Cycling: The working electrodes consisted of 90 wt.% graphite powder (MTI Corp.) and 10 wt.% PVDF binder (poly(vinylidene difluoride) from PI-KEM Ltd). NMP (*N*-methylpyrrolidone from Sigma–Aldrich) was used as solvent to form the slurries that were cast onto carbon coated copper current collectors. The electrode sheets were dried at room temperature overnight, punched into electrodes, and dried again under vacuum overnight at 110 °C. For galvanostatic cycling, CR2032 coin cells (MTI Corp.) were assembled with electrodes of 12 mm diameter with an average thickness of 120 µm. The average mass of the electrodes used was 28.8 mg with 16.8 mg active material. The cell assembly was performed in an argon filled glovebox from MBraun (H_2O < 0.1 ppm, O_2 < 0.1 ppm). Na metal (BASF) was used as the counter electrode and a Whatman membrane (GF/A) as the separator with a desired volume of electrolyte.

For the electrolyte preparation, sodium bis(trifluoromethanesulfonyl)imide (NaTFSI purity 99.5%, Solvionic) and sodium hexafluorophosphate ($NaPF_6$, purity > 99.5%, E-lyte) were used as salt. Monoglyme (G1, Sigma–Aldrich) and diglyme (G2, Sigma–Aldrich) were pre-dried with 4 Å porous molecular sieves overnight. The electrochemical galvanostatic charge discharge experiments were conducted using a BCS 805 battery cycler from Biologic at a current of C/10 (1C = 110 mA g^{-1}).

Experimental Methods: The mass change experiments were conducted in several ways. First, we reproduced the results by Kim et al., these measurements were carried out as described by the authors, see Supporting Information for details.[2b] New mass change measurement were carried out following our updated protocol: First, a graphite electrode was sodiated, at constant current, in a coin cell to a specific potential (or SOS). Then it was desodiated at 2 V and finally sodiated at the desire potential where it was held for a minimum of 6 h. These samples were henceforth referred to as sodiated samples. For each sodiated sample, a desodiated control sample was prepared. This was done by applying the same cycling protocol but adding a desodiation step at the end (sample held at 2 V over at least 6 h at the end). All the cells were taken to an Ar-filled glove box and were disassembled. Immediately after a cell was opened, the graphite electrode was carefully peeled from the separator and placed in a weighing boat in order to measure the mass on a Pioneer PX225D balance with a readability of 0.01 mg.

Electrochemical impedance spectroscopy (EIS) experiments were carried out to determine the electrolyte concentration at different sodiation stages during the co-intercalation process. The electrochemical set up was prepared in a similar way to described before. The coin cells were probed via EIS using a potentiostat (MPG-3 from Biologic) in the frequency range of 20 kHz–1 Hz. In the high frequency region, the impedance response showed a low reactance and thus might be interpreted as a high frequency resistance (HFR) that is mainly dominated by the conductivity of the bulk electrolyte and the contact resistance.[18] Thus, this HFR was used for the determination of the concentration during cycling at a frequency of 20 kHz where the samples showed the lowest imaginary part. To correlate the determined HFR of the in situ measurements with an electrolyte concentration, calibration measurements were carried out for assembled cells with various electrolyte concentrations after 6 h of equilibration and conducting a single sodiation step (0.1 C, 10 min). For the determination of the HFR at various states of sodiation, the sample was sodiated with a constant discharge current pulse of 0.1 C for 10 min. Subsequently the respective potential was kept for 5 min and the impedance measurement were conducted. This sequence was repeated until a final cell potential of 0.01 V versus Na^+/Na was reached.

For the operando optical microscopy, an EL-Cell ECC Opto-10 cell holder with a two-electrode side-by-side arrangement of the graphite electrode stripe and metallic counter electrode stripe were used. The cells were cycled at 0.1 C. A digital optical microscope (Keyence VHX-7000) with a 500x magnification was used and an image was taken every 120 s.

Computational Methods: Gaussian 16 was used to optimize 2 solvation shells where Na^+ is fully solvated by either 2 G2, or by 6 PC molecules to compare with a standard carbonate-based electrolyte. The structures were optimized at the B3LYP/6-311+G(d,p) level of theory with the SMD implicit solvent model, setting the dielectric constant to 7.23 and 64 for G2 and PC, respectively.[7j,19] A full populations analysis was carried out along with a calculation of the electric field potential using the Gaussian 16 cubegen tool.[19a] The average potential energy as a function of distance to the cation was computed by averaging over a sphere centred around the cation. Similarly, the average electric potential in a particular direction from the cation was computed by averaging the electric potential along spherical solid angles, which was then projected on a 2D surface using the area preserving Mollweide projection.[20]

To study the structure and stability of the solvation shell we performed ab initio molecular dynamics using Car-Parrinello molecular dynamics (CPMD).[21] 1 M $NaPF_6$ in G2 was simulated. A cubic unit cells was constructed (4 $NaPF_6$ with 28 G2, randomly distributed) in Packmol with side 19.095 Å. G2 exists in several possible confirmations, several conformations were optimized in Gaussian 16 and the 7 most energetically stable were used as starting structures in the MD simulation. A plane-wave cut-off of 90 Rydberg and a time step of 4 a. u., and the PBE functional was used,[22] along with pseudopotential of Goedecker, Teter and Hutter, for all species except for Na where the pseudopotential of Troullier and Martins was used.[23] A Nosé-Hoover thermostat was switched on after equilibrating the system. The temperature was set at 300 K. Subsequently a 40 ps production runs was carried out. The content of the solvation shell was studied by computing the (partial) radial distribution functions (RDFs) from the production trajectory:

$$g_i(r) = \frac{n_i(r)}{4\pi r^2 \Delta r} \frac{1}{\rho_i} \qquad (4)$$

where $n_i(r)$ is the average number of atoms of type i in a spherical shell with thickness Δr at distance r from the central cation, and ρ_i is the average number density of atom of type i. By integrating the partial RDFs, the coordination number was computed. All solvents and anions where also replaced by their center of mass and new RDFs were computed with respect to the center of mass in order to study the number of solvents and anions in the solvation shell. By integrating the Na^+-CM partial RDFs the solvation number is acquired.[14h]

Full solvation shells [Na:G2$_2$]$^+$ in a graphitic host consisting of 32 AB stacked carbon atoms was studied using the Vienna ab initio simulation package (VASP) with an plane-wave energy cut-off at 520 eV,

corresponding to $1.3 \times$ ENMAX of the maximum energy in the pseudopotentials, using a [4,4,4] gamma centered k-point sampling mesh and the PBE functional.[22,24] Similarly, LiC_6 was simulated. The structures where relaxed using ISIF = 3, i.e., both ions and unit cell shape and volume was allowed to relax. Band structure calculations were carried out along the $\Gamma - M - K - \Gamma - A - L - H - A$ k-point path, for both $[Na:G2_2]C_{32}$ and LiC_6, typical of hexagonal structures.

The charge density difference $\Delta\rho$ was computed:

$$\Delta\rho = \rho_{system} - \rho_{SS} - \rho_{Gr} \tag{5}$$

where ρ_{system} is the electron density of the neutral system, ρ_{SS} is the electron density of the positively charged solvation shell and ρ_{Gr} is the electron density of the negatively charged expanded graphite structure.

Supporting Information

Supporting Information is available from the Wiley Online Library or from the author.

Conflict of Interest

The authors declare no conflict of interest.

Data Availability Statement

The data that support the findings of this study are available from the corresponding author upon reasonable request.

[1] a) B. Jache, P. Adelhelm, *Angew. Chem., Int. Ed.* **2014**, *53*, 10169; b) H. Kim, J. Hong, Y.-U. Park, J. Kim, I. Hwang, K. Kang, *Adv. Funct. Mater.* **2015**, *25*, 534.

[2] a) I. Escher, Y. Kravets, G. A. Ferrero, M. Goktas, P. Adelhelm, *Energy Technology* **2021**, *9*, 2000880; b) H. Kim, J. Hong, G. Yoon, H. Kim, K.-Y. Park, M.-S. Park, W.-S. Yoon, K. Kang, *Energy Environ. Sci.* **2015**, *8*, 2963; c) L. Seidl, N. Bucher, E. Chu, S. Hartung, S. Martens, O. Schneider, U. Stimming, *Energy Environ. Sci.* **2017**, *10*, 1631.

[3] T. Palaniselvam, B. Babu, H. Moon, I. Hasa, A. L. Santhosha, M. Goktas, Y.-N. Sun, L. Zhao, B.-H. Han, S. Passerini, A. Balducci, P. Adelhelm, *Batteries Supercaps* **2021**, *4*, 173.

[4] a) B. Jache, J. O. Binder, T. Abe, P. Adelhelm, *Phys. Chem. Chem. Phys.* **2016**, *18*, 14299; b) H. Zhang, Z. Li, W. Xu, Y. Chen, X. Ji, M. M. Lerner, *Nanotechnology* **2018**, *29*, 325402.

[5] a) G. A. Ferrero, G. Åvall, K. A. Mazzio, Y. Son, K. Janßen, S. Risse, P. Adelhelm, *Adv. Energy Mater.* **2022**, *12*, 2202377; b) J. Park, S. J. Kim, K. Lim, J. Cho, K. Kang, *ACS Energy Lett.* **2022**, *7*, 3718.

[6] a) J. O. Besenhard, *Carbon* **1976**, *14*, 111; b) N. Okuyama, T. Takahashi, S. Kanayama, H. Yasunaga, *Physica B+C* **1981**, *105*, 298; c) J. O. Besenhard, H. P. Fritz, *Angew. Chem. Int. Ed. Engl.* **1983**, *22*, 950.

[7] a) J. O. Besenhard, H. P. Fritz, *J. Electroanal. Chem. Interfacial Electrochem.* **1974**, *53*, 329; b) M. Arakawa, J.-I. Yamaki, *J. Electroanal. Chem. Interfacial Electrochem.* **1987**, *219*, 273; c) J. O. Besenhard, M. Winter, J. Yang, W. Biberacher, *J. Power Sources* **1995**, *54*, 228; d) G. C. Chung, H. J. Kim, S. I. Yu, S. H. Jun, J. w. Choi, M. H. Kim, *J. Electrochem. Soc.* **2000**, *147*, 4391; e) M. R. Wagner, J. H. Albering, K. C. Moeller, J. O. Besenhard, M. Winter, *Electrochem. Commun.* **2005**, *7*, 947; f) Y.-O. Kim, S.-M. Park, *J. Electrochem. Soc.* **2001**, *148*, A194; g) K. Xu, *Chem. Rev.* **2004**, *104*, 4303; h) M. Winter, *Mater. Sci.* **2009**, *223*, 1395; i) S. J. An, J. Li, C. Daniel, D. Mohanty, S. Nagpure, D. L. Wood, *Carbon* **2016**, *105*, 52; j) K. Xu, *Chem. Rev.* **2014**, *114*, 11503.

[8] a) M. Hahn, H. Buqa, P. W. Ruch, D. Goers, M. E. Spahr, J. Ufheil, P. Novák, R. Kötz, *Electrochem. Solid-State Lett.* **2008**, *11*, A151; b) M. E. Spahr, T. Palladino, H. Wilhelm, A. Würsig, D. Goers, H. Buqa, M. Holzapfel, P. Novák, *J. Electrochem. Soc.* **2004**, *151*, A1383.

[9] a) J. Chmiola, G. Yushin, Y. Gogotsi, C. Portet, P. Simon, P. L. Taberna, *Science* **2006**, *313*, 1760; b) P. Simon, Y. Gogotsi, B. Dunn, *Science* **2014**, *343*, 1210; c) S. Fleischmann, Y. Zhang, X. Wang, P. T. Cummings, J. Wu, P. Simon, Y. Gogotsi, V. Presser, V. Augustyn, *Nat. Energy* **2022**, *7*, 222.

[10] L. Borchardt, D. Leistenschneider, J. Haase, M. Dvoyashkin, *Adv. Energy Mater.* **2018**, *8*, 1800892.

[11] a) J. Park, Z.-L. Xu, K. Kang, *Front Chem.* **2020**, *8*, 432; b) Z. Zhu, F. Cheng, Z. Hu, Z. Niu, J. Chen, *J. Power Sources* **2015**, *293*, 626; c) A. P. Cohn, K. Share, R. Carter, L. Oakes, C. L. Pint, *Nano Lett.* **2016**, *16*, 543.

[12] J. O. Besenhard, H. Möhwald, J. J. Nickl, *Carbon* **1980**, *18*, 399.

[13] a) J. Park, Z.-L. Xu, G. Yoon, S. K. Park, J. Wang, H. Hyun, H. Park, J. Lim, Y.-J. Ko, Y. S. Yun, K. Kang, *Adv. Mater.* **2020**, *32*, 1904411; b) S. J. Richard Prabakar, A. B. Ikhe, W. B. Park, K.-C. Chung, H. Park, K.-J. Kim, D. Ahn, J. S. Kwak, K.-S. Sohn, M. Pyo, *Adv. Sci.* **2019**, *6*, 1902129; c) L. Li, L. Liu, Z. Hu, Y. Lu, Q. Liu, S. Jin, Q. Zhang, S. Zhao, S.-L. Chou, *Angew. Chem., Int. Ed.* **2020**, *59*, 12917.

[14] a) L. Troxler, G. Wipff, *J. Am. Chem. Soc.* **1994**, *116*, 1468; b) E. M. Cabaleiro-Lago, M. A. Ríos, *Chem. Phys.* **1998**, *236*, 235; c) D. Spångberg, K. Hermansson, *Chem. Phys.* **2004**, *300*, 165; d) G. Kamath, R. W. Cutler, S. A. Deshmukh, M. Shakourian-Fard, R. Parrish, J. Huether, D. P. Butt, H. Xiong, S. K. R. S. Sankaranarayanan, *J. Phys. Chem. C* **2014**, *118*, 13406; e) M. He, K. C. Lau, X. Ren, N. Xiao, W. D. McCulloch, L. A. Curtiss, Y. Wu, *Angew. Chem., Int. Ed.* **2016**, *55*, 15310; f) A. V. Cresce, S. M. Russell, O. Borodin, J. A. Allen, M. A. Schroeder, M. Dai, J. Peng, M. P. Gobet, S. G. Greenbaum, R. E. Rogers, K. Xu, *Phys. Chem. Chem. Phys.* **2017**, *19*, 574; g) E. Flores, G. Åvall, S. Jeschke, P. Johansson, *Electrochim. Acta* **2017**, *233*, 134; h) G. Åvall, P. Johansson, *J. Chem. Phys.* **2020**, *152*, 234104; i) G. Åvall, J. Mindemark, D. Brandell, P. Johansson, *Adv. Energy Mater.* **2018**, *8*, 1703036; j) M. Okoshi, C.-P. Chou, H. Nakai, *J. Phys. Chem. B* **2018**, *122*, 2600; k) D. Monti, E. Jónsson, A. Boschin, M. R. Palacín, A. Ponrouch, P. Johansson, *Phys. Chem. Chem. Phys.* **2020**, *22*, 22768.

[15] a) N. Leifer, M. F. Greenstein, A. Mor, D. Aurbach, G. Goobes, *J. Phys. Chem. C* **2018**, *122*, 21172; b) I. Escher, A. I. Freytag, J. M. Lopez del Amo, P. Adelhelm, *Batteries & Supercaps* **2023**, *6*, e202200421; c) K.

**ADVANCED
SCIENCE NEWS**

www.advancedsciencenews.com

**ADVANCED
ENERGY
MATERIALS**

www.advenergymat.de

Gotoh, H. Maruyama, T. Miyatou, M. Mizuno, K. Urita, H. Ishida, *J. Phys. Chem. C* **2016**, *120*, 28152.

[16] Z. L. Xu, G. Yoon, K. Y. Park, H. Park, O. Tamwattana, S. Joo Kim, W. M. Seong, K. Kang, *Nat. Commun.* **2019**, *10*, 2598.

[17] a) M. Goktas, C. Bolli, E. J. Berg, P. Novák, K. Pollok, F. Langenhorst, M. v. Roeder, O. Lenchuk, D. Mollenhauer, P. Adelhelm, *Adv. Energy Mater.* **2018**, *8*, 1702724; b) M. Goktas, C. Bolli, J. Buchheim, E. J. Berg, P. Novák, F. Bonilla, T. Rojo, S. Komaba, K. Kubota, P. Adelhelm, *Applied Materials and Interfaces* **2019**, *11*, 32844.

[18] W. Choi, H.-C. Shin, J. M. Kim, J.-Y. Choi, W.-S. Yoon, *J. Electrochem. Sci. Technol.* **2020**, *11*, 1.

[19] a) M. J. Frisch, G. W. Trucks, H. B. Schlegel, G. E. Scuseria, M. A. Robb, J. R. Cheeseman, G. Scalmani, V. Barone, G. A. Petersson, H. Nakatsuji, X. Li, M. Caricato, A. V. Marenich, J. Bloino, B. G. Janesko, R. Gomperts, B. Mennucci, H. P. Hratchian, J. V. Ortiz, A. F. Izmaylov, J. L. Sonnenberg, F. D. Williams, F. Lipparini, F. Egidi, J. Goings, B. Peng, A. Petrone, T. Henderson, D. Ranasinghe, V. G. Zakrzewski, et. al., Wallingford, C T, **2016**; b) A. D. Becke, *J. Chem. Phys.* **1993**, *98*, 5648; c) A. D. Becke, *Phys. Rev. A* **1988**, *38*, 3098; d) C. Lee, W. Yang, R. G. Parr, *Phys. Rev. B* **1988**, *37*, 785; e) A. V. Marenich, C. J. Cramer, D. G. Truhlar, *J. Phys. Chem. B* **2009**, *113*, 6378.

[20] J. P. Snyder, in *Professional Paper*, Washington, D.C **1987**.

[21] R. Car, M. Parrinello, *Phys. Rev. Lett.* **1985**, *55*, 2471.

[22] J. P. Perdew, K. Burke, M. Ernzerhof, *Phys. Rev. Lett.* **1996**, *77*, 3865.

[23] a) N. Troullier, J. L. Martins, *Phys. Rev. B* **1991**, *43*, 1993; b) S. Goedecker, M. Teter, J. Hutter, *Phys. Rev. B* **1996**, *54*, 1703; c) C. Hartwigsen, S. Goedecker, J. Hutter, *Phys. Rev. B* **1998**, *58*, 3641.

[24] a) G. Kresse, J. Furthmüller, *Comput. Mater. Sci.* **1996**, *6*, 15; b) G. Kresse, J. Furthmüller, *Phys. Rev. B* **1996**, *54*, 11169; c) G. Kresse, J. Furthmüller, J. Hafner, *Phys. Rev. B* **1994**, *50*, 13181; d) G. Kresse, J.

Hafner, *Phys. Rev. B* **1993**, *47*, 558; e) G. Kresse, D. Joubert, *Phys. Rev. B* **1999**, *59*, 1758.

[25] P. N. Le Pham, V. Gabaudan, A. Boulaoued, G. Åvall, F. Salles, P. Johansson, L. Monconduit, L. Stievano, *Energy Storage Mater.* **2022**, *45*, 291.

[26] a) H. J. Kim, Y. Park, Y. Kwon, J. Shin, Y.-H. Kim, H.-S. Ahn, R. Yazami, J. W. Choi, *Energy Environ. Sci.* **2020**, *13*, 286; b) H. Wang, S. C. Kim, T. Rojas, Y. Zhu, Y. Li, L. Ma, K. Xu, A. T. Ngo, Y. Cui, *J. Am. Chem. Soc.* **2021**, *143*, 2264.

[27] M. W. Chase, N. I. S. Organization, *American Chemical Society*, Washington, DC, **1998**.

[28] a) P. Maire, A. Evans, H. Kaiser, W. Scheifele, P. Novák, *J. Electrochem. Soc.* **2008**, *155*, A862; b) S. J. Harris, A. Timmons, D. R. Baker, C. Monroe, *Chem. Phys. Lett.* **2010**, *485*, 265; c) F. Grimsmann, T. Gerbert, F. Brauchle, A. Gruhle, J. Parisi, M. Knipper, *J. Energy Storage* **2018**, *15*, 17; d) Y. Chen, K.-H. Chen, A. J. Sanchez, E. Kazyak, V. Goel, Y. Gorlin, J. Christensen, K. Thornton, N. P. Dasgupta, *J. Mater. Chem. A* **2021**, *9*, 23522.

[29] R. Andersson, F. Årén, A. A. Franco, P. Johansson, *J. Comput. Chem.* **2021**, *42*, 1632.

[30] a) R. Andersson, F. Årén, A. A. Franco, P. Johansson, *J. Electrochem. Soc.* **2020**, *167*, 140537; b) D. M. Seo, O. Borodin, D. Balogh, M. O'Connell, Q. Ly, S.-D. Han, S. Passerini, W. A. Henderson, *J. Electrochem. Soc.* **2013**, *160*, A1061; c) B. Bagchi, B. Jana, *Chem. Soc. Rev.* **2010**, *39*, 1936; d) V. S. Smirnov, S. A. Kislenko, *ChemPhysChem* **2018**, *19*, 75.

[31] J. Rouquerol, D. Avnir, C. W. Fairbridge, D. H. Everett, J. M. Haynes, N. Pernicone, J. D. F. Ramsay, K. S. W. Sing, K. K. Unger, *Pure Appl. Chem.* **1994**, *66*, 1739.

[32] S. C. Jung, Y. J. Kang, Y. K. Han, *Nano Energy* **2017**, *34*, 456.

2301944 (13 of 13)